Supplementary Information for

Synergistic elimination of antibiotic resistance genes and tetracycline antibiotics in wastewater via a Z-scheme Bi_2WO_6/g-C_3N_4 heterojunction: Degradation pathways and mechanism

Yuankun Liu[a*], Gangyi Sun [a], Yuanqi Cao[a], Xing Li[a], Zhangya Li[a], Zhonglin Chen[b*]

[a] College of Architecture and Civil Engineering, Beijing University of Technology, Beijing 100124, P.R. China

[b] State Key Laboratory of Urban-rural Water Resources and Environment, Harbin Institute of Technology, Harbin 150090, P. R. China

***Corresponding author:**

E-mail: liuyuankun@bjut.edu.cn (Yuankun Liu)

Supplementary data

Text S1. Main experimental materials

Melamine (99.0% purity, $C_3H_6N_6$), bismuth nitrate pentahydrate (99.0% purity, BiN_3O_9-$5H_2O$), disodium ethylenediaminetetraacetate (99.0% purity, EDTA-2Na), aureomycin hydrochloride ($C_{22}H_{23}ClN_2O_8$-HCl), isopropyl alcohol (IPA), anhydrous ethanol (99.7% purity), sodium chloride (99.5% purity, NaCl), sodium bicarbonate (99.8% purity, $NaHCO_3$) and sodium sulfate (99.0% purity, Na_2SO_4) were purchased from Aladdin Industries (Shanghai, China). 5,5-Dimethyl-1-pyrroline-N-oxide (97.0% purity, DMPO) was purchased from Sigma, USA. Sodium tungstate dihydrate (98.0% purity, $H_4Na_2O_6W$) and hexadecyltrimethylammonium bromide (98.0% purity, CTAB) were procured from Bide Pharmaceuticals Ltd (Shanghai, China). Tetracycline (98.0% purity, $C_{22}H_{24}N_2O_8$, Myriad, Beijing), oxytetracycline hydrochloride (95.0% purity, $C_{22}H_{24}N_2O_9$-HCl, Maclean's, Shanghai) and azoxypiperidinol (98.0% purity, Tempol, Leyan) were also used. All the remaining reagents were of analytical-grade quality and procured from the Beijing Chemical Plant (Beijing, China). All reagents were employed without undergoing further purification. Ultrapure water was used for the preparation of all aqueous solutions. (Milli-Q A10, Millica, MA, USA). The water from Longtan Lake (Beijing, China) was collected to simulate the actual water quality, filtered through a 0.45 μm membrane, and then stored in a refrigerator at 4° C.

Text S2. Preparation of g-C_3N_4

The g-C_3N_4 was fabricated in accordance with the previously documented method[1]. A specific quantity of melamine was weighed and then positioned within a tube furnace. It was heated up to 520 °C with a heating rate of 2.3 °C/min and kept for 4 h. After cooling to room temperature, the resulting g-C_3N_4 was ground into powder for later use. The first calcination product was then subjected to a second calcination in the tube furnace. The heating rate was set to 5 °C/min, and the temperature was raised to 500 °C and maintained for 2 h. After cooling to room temperature and thorough grinding, a light-yellow g-C_3N_4 sample was obtained.

Text S3. Preliminary optimization experiments

Preliminary experiments were conducted to optimize the synthesis parameters of the Bi_2WO_6/g-C_3N_4 composite. As shown in Fig S1, the photocatalytic performance was significantly influenced by the Bi_2WO_6 loading, precursor solution pH, and calcination temperature (TC = 20 mg/L, catalyst dosage = 0.2 g/L). The optimal photocatalytic activity was obtained at a Bi_2WO_6 content of 15 wt%, which can be attributed to the formation of sufficient heterojunction interfaces, while excessive loading caused particle agglomeration and reduced active sites. The precursor solution pH also affected the nucleation and growth of Bi_2WO_6, and the sample prepared at pH 3 exhibited enhanced activity due to more uniform crystal growth. In addition, the calcination temperature played an important role in determining the crystallinity and surface properties of the composite, with 160 °C identified as the optimal temperature. Under these conditions, the TC removal efficiency reached 81.80%. Therefore, a Bi_2WO_6/g-C_3N_4 mass ratio of 15 wt%, synthesis pH of 3, and calcination temperature of 160 °C were selected for subsequent experiments.

Text S4. Characterization

The morphological characteristics and microstructure of the samples were observed by means of scanning electron microscopy (SEM, Hitachi SU9000) as well as field emission transmission electron microscopy (TEM, JEOLJEM 2100F, accelerating voltage 200 kV).The crystal structure and material composition of the samples were analyzed using X-ray diffraction (XRD, D8 ADVANCE, Bruker, Germany) The specific surface area and pore size distribution characteristics of the materials were determined using a physisorption instrument (ASAP 2460, Mack Corporation, USA). A UV-visible-NIR spectrophotometer (UV-vis DRS, UV3600, Shimadzu, Japan) was employed to record the UV-visible diffuse reflectance spectra of the samples. X-ray photoelectron spectrometry (XPS, Thermo ESCALAB 250Xi, Thermo Fisher, USA) was utilized to analyze the surface elemental composition and valence band structure of the samples. The functional groups on the sample surface were determined by Fourier infrared spectrometry (FT-IR, Thermo NICOLET6700). A fluorescence spectrometer (FLS1000/FS5, Edinburgh, UK) was employed to analyze the electron migration and complexation processes of the samples.

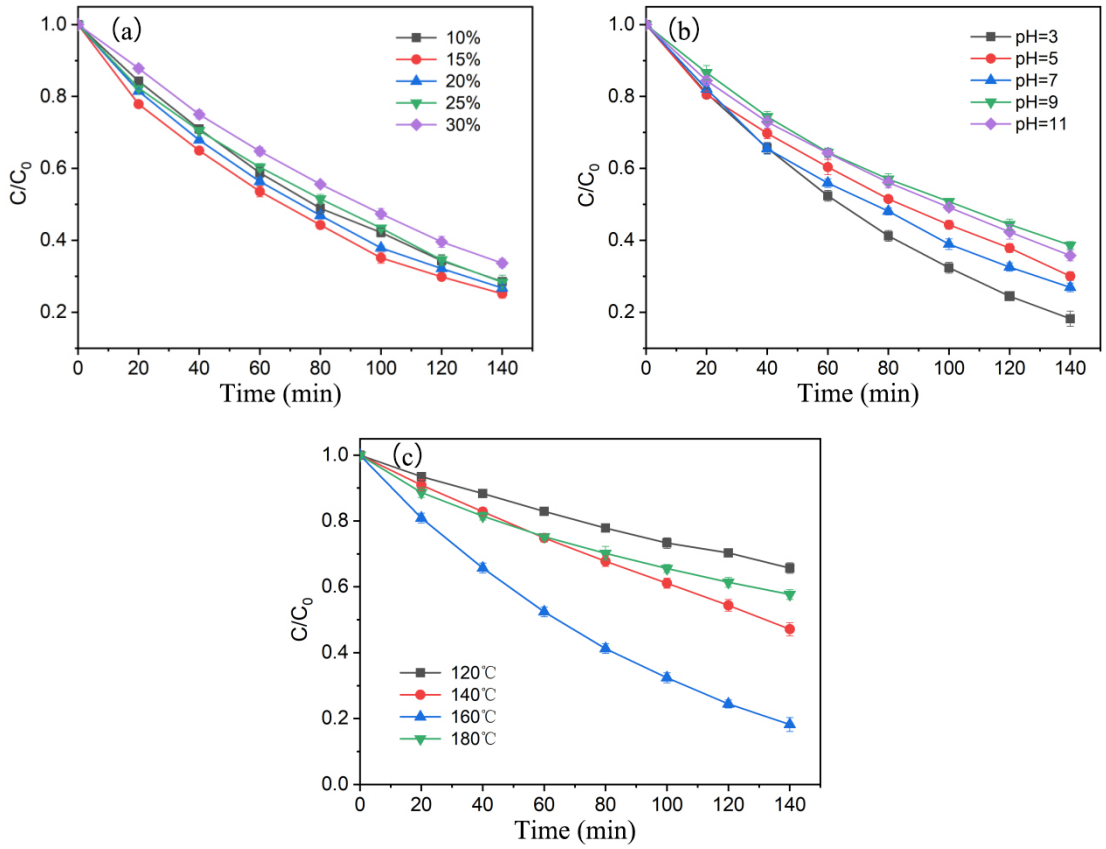

Figure S1.(a) Bi_2WO_6/g-C_3N_4 photocatalytic oxidation removal rates at different mass ratios, (b) at different pH values, and (c) at different calcination temperatures

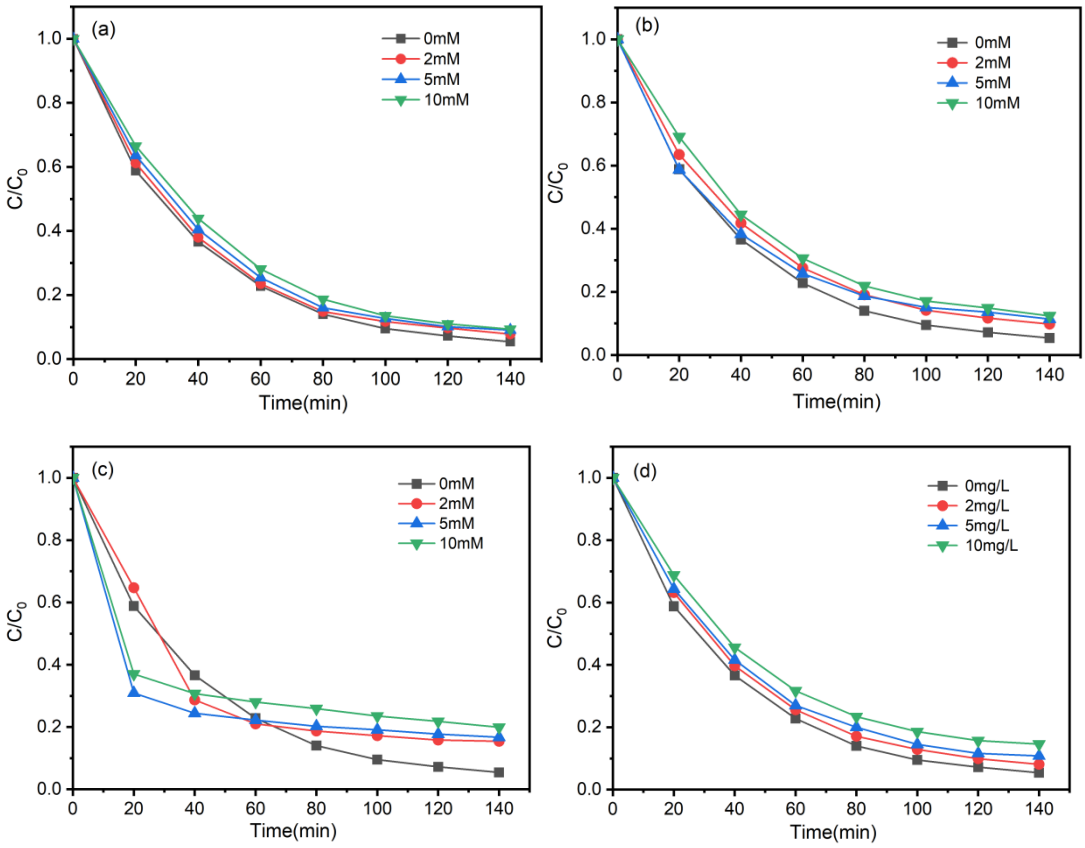

Figure S2. Effects of (a) Cl^-, (b) SO_4^{2-} , (c) HCO_3^- and (d) HA on the photocatalytic degradation of TC by Bi_2WO_6/g-C_3N_4.

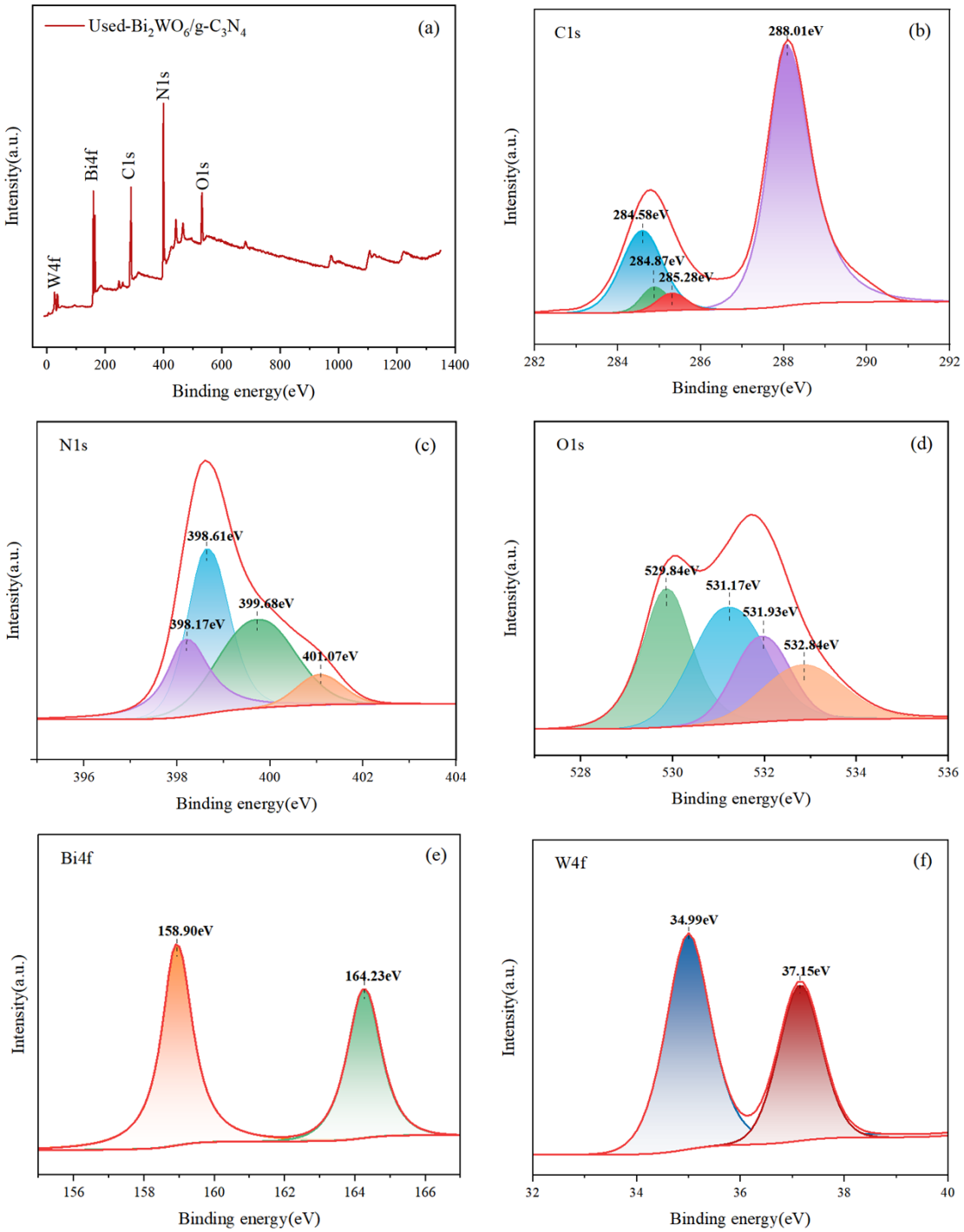

Figure S3. X-ray Photoelectron (a) Survey, (b) C1s, (c) N1s, (d) O1s, (e) Bi4f and (f) W4f spectrum of Used-Bi_2WO_6/g-C_3N_4

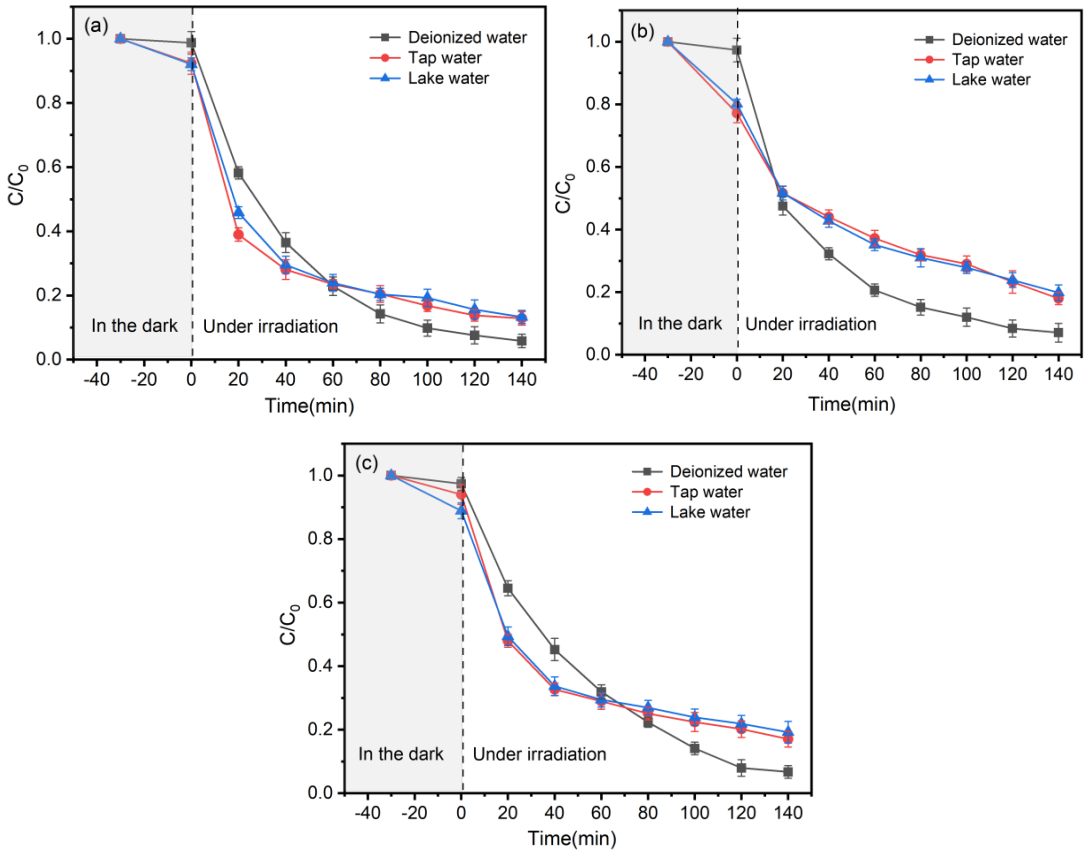

Figure S4. Photocatalytic degradation of (a) TC, (b) CTC and (c) OTC in deionized water, tap water and lake water.

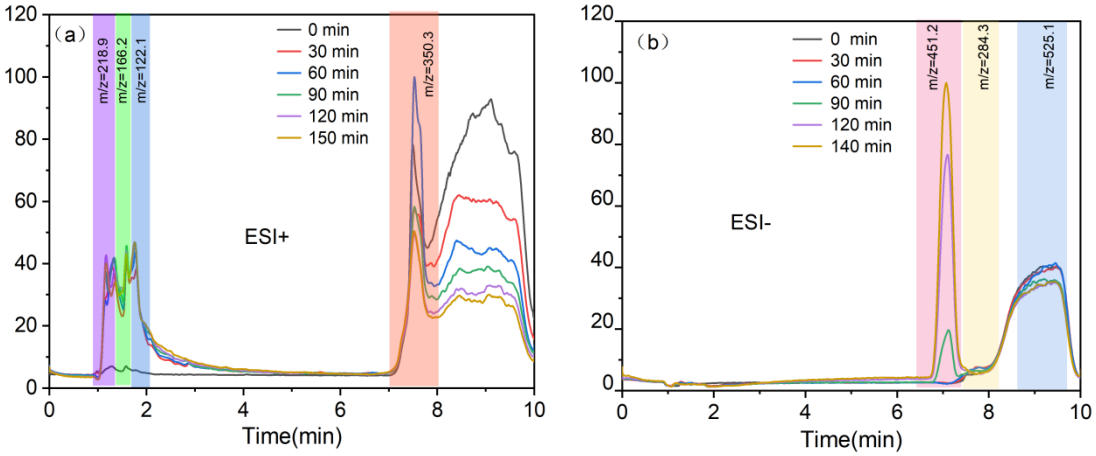

Figure S5. Liquid chromatogram of photocatalytic oxidation of TC.

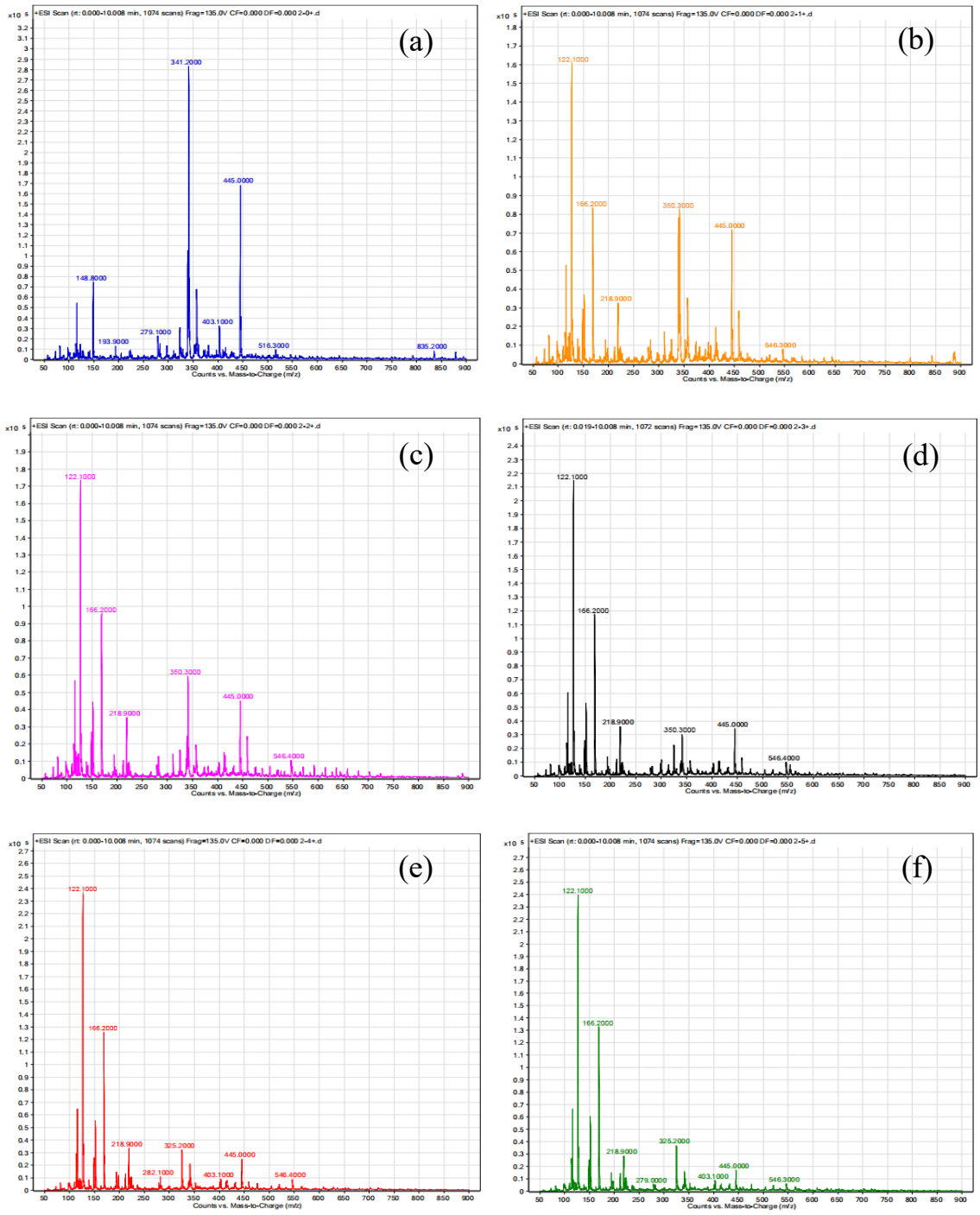

Figure S6. Liquid-phase mass spectra of photocatalytic oxidation of TC in ESI+ mode.

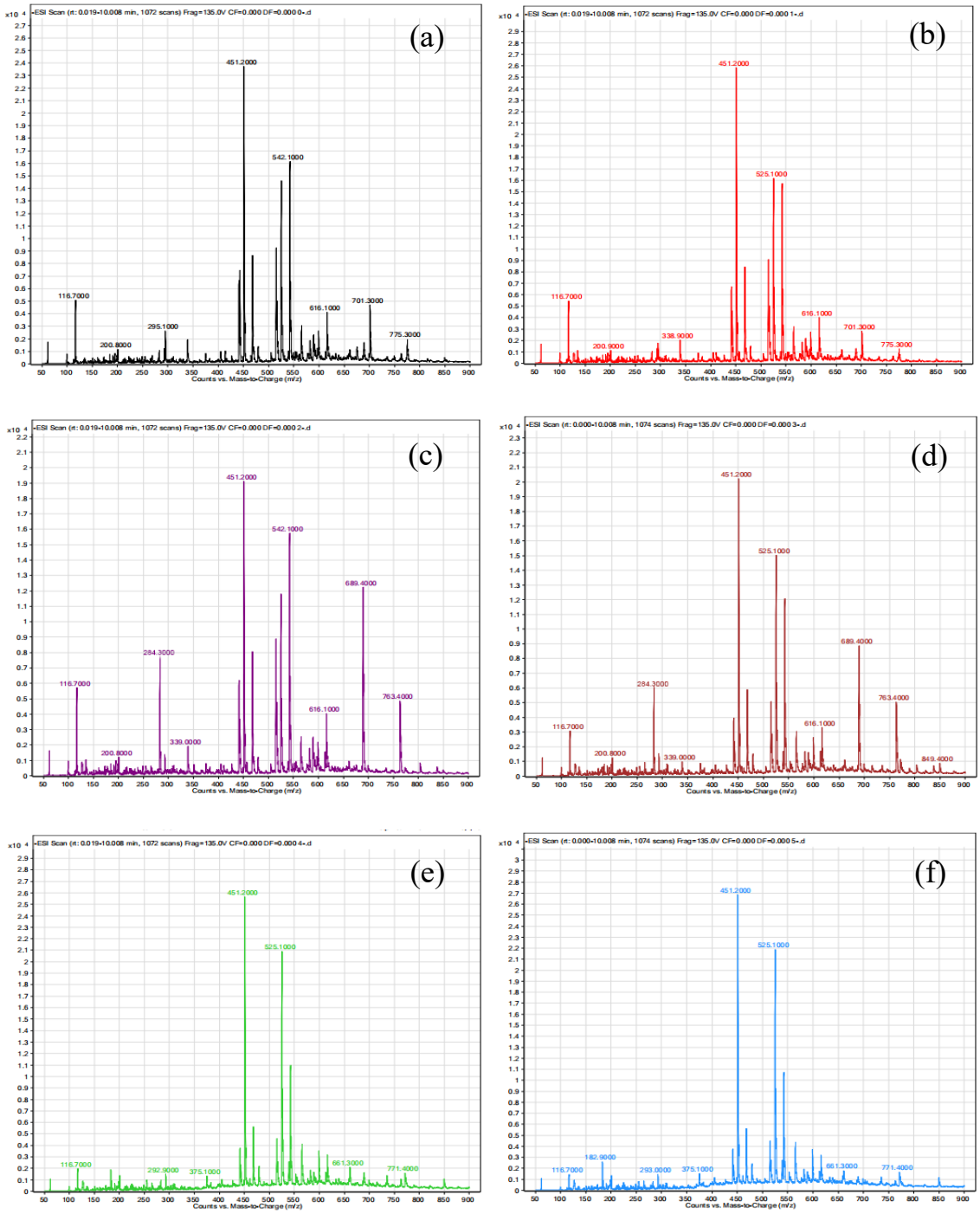

Figure S7. Liquid-phase mass spectra of photocatalytic oxidation of TC in ESI-mode.

Table S1. Main water quality indicators of the real water.

Parameter	Tap water	Lake water
pH	7.15 ± 0.20	7.20 ± 0.20
Turbidity (NTU)	0.405 ± 0.08	1.055 ± 0.05
DOC (mg L^{-1})	1.171 ± 0.20	2.515 ± 0.40
UV_{254} (cm^{-1})	0.0200 ± 0.004	0.0587 ± 0.007

Table S2. The qPCR reaction system.

Components	**Volume（μL）**
1×LightCycler 480 SYBR Gree I Master	10
PCR Forwad primer(10 μM)	1
PCR Reverse primer(10 μM)	1
DNA template	2
ddH_2O	6
Total Volume	20

Table S3. Upstream and downstream primers.

Target genes	Primer	Sequence	Amplified fragments /bp	Annealing temperature /℃
tet A	F	CTCACCAGCCTGACCTCGAT	210	61
	R	CACGTTGTTATAGAAGCCGCATAG		
tet C	F	ACTGGTAAGGTAAACGCCATTGTC	418	68
	R	ATGCATAAACCAGCCATTGAGTAAG		
sulI	F	GCCGATGAGATCAGACGTATTG	162	60
	R	CGCATAGCGCTGGGTTTC		
sulII	F	TCATCTGCCAAACTCGTCGTTA	191	59
	R	GTCAAAGAACGCCGCAATGT		
intI1	F	GCCTTGATGTTACCCGAGAG	280	60
	R	GATCGGTCGAATGCGTGT		
16S rRNA	F	GGGTTGCGCTCGTTGC	193	55
	R	ATGGYTGTCGTCAGCTCGTG		

Table S4. qPCR reaction procedure.

Procedure	Temperature(℃)	Time	Remark
Pre-denaturation	95	10 min	
Denaturation	95	30 s	Denaturation to extension 40 cycles in
Annealing	60	30 s	total.
Extension	72	30 s	

Table S5. The physical and chemical parameters of photocatalytic materials.

Samples	S_{BET}(m^2/g)	Average Pore diameter(nm)	Pore Volume(cm^3/g)
g-C_3N_4	8.052	22.034	0.044
Bi_2WO_6/g-C_3N_4	46.430	13.083	0.152

Table S6. The proposed first-order kinetic parameters of different photocatalytic materials.

Catalyst types	TC		CTC		OTC	
	K	**R^2**	**K**	**R^2**	**K**	**R^2**
g-C_3N_4	0.00808	0.9929	0.01009	0.9975	0.00299	0.9779
Bi_2WO_6	0.00533	0.9993	0.00924	0.9266	0.00909	0.9973
Bi_2WO_6/g-C_3N_4	0.02047	0.9853	0.01784	0.9668	0.0197	0.9928

Table S7. Comparison of catalyst stability during degradation between Bi_2WO_6/g-C_3N_4 and previously reported photocatalysts.

Photocatalyst System	Target pollutant	Number of cycles	Stability	References
N-TiO_2/g-C_3N_4	RhB	5	82.3% retained	[2]
Bare Ag_3PO_4	MB/RhB	6	50% retained	[3]
Cu-MOF	Reactive Blue	5	83.3% retained	[4]
TPP/ AgBr	Rhb	3	80% retained	[5]
CuO-NiO	cefixime	5	78% retained	[6]
$BaTiO_3$ (T-Ba)	ciprofloxacin	5	47% retained	[7]
CdS/PANI/MWCNTs	SBX	5	84.6% retained	[8]
Bi_2WO_6/g-C_3N_4	TC	5	85.49% retained	This work

Table S8. Chemical formulas and main fragments (m/z) of intermediate products.

ID	m/z	Chemical Formula	Proposed Structure
A	476.4	$C_{22}H_{24}O_{10}N_2$	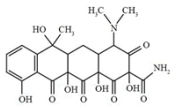
B	350.3	$C_{17}H_{20}O_7N$	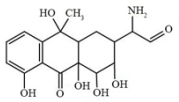
C	284.3	$C_{15}H_{24}O_5$	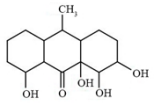
D	416.4	$C_{20}H_{20}O_8N_2$	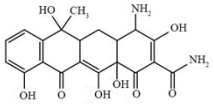
E	318.3	$C_{16}H_{14}O_7$	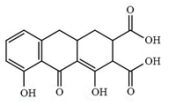
F	218.2	$C_{12}H_{10}O_4$	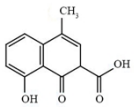
G	122.1	$C_7H_6O_2$	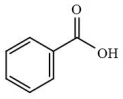
H	166.2	$C_9H_{10}O_3$	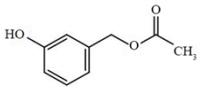

References

[1] Y. Zhou, Y. Zhang, M. Lin, J. Long, Z. Zhang, H. Lin, J.C. Wu, X. Wang, Monolayered Bi_2WO_6 nanosheets mimicking heterojunction interface with open surfaces for photocatalysis, Nat Commun 6 (2015) 8340.https://10.1038/ncomms9340

[2] R. Liu, M. Li, J. Chen, Y. Yin, W. Zhao, Z. Gong, H. Jin, Z. Liu, Enhanced photocatalytic degradation of tetracycline by magnetically separable g-C_3N_4-doped magnetite@titanium dioxide heterostructured photocatalyst, Water 16 (2024) 1372. https://doi.org/10.3390/w16101372

[3] P. Kavya, S. Priya, K. Pradeesh, K. Sandeep, K. P. Saranya, V. L. Thomas, M. Shanthil, Thin silica shell on Ag_3PO_4 nanoparticles augments stability and photocatalytic reusability, RSC Adv , 13 (2023) 30643–30648.https://doi.org/10.1039/D3RA05023H

[4] Z.A. Suliman, A.A. Ibrahim, C.A. Mecha, M.N. Chollom, Photocatalytic degradation and antibacterial efficacy of novel synthesized green Cu–Fe metal organic framework derived from Acacia nilotica extract, Discover Chemistry 2 (2025) 219.https://doi.org/10.1007/s44371-025-00297-7

[5] Z. Song, H. Ma, J. Lu, G. Huang, Q. Gao, C. Xiao, Enhanced TPP/AgBr photocatalysis with Z-scheme heterojunctions for degradation of RhB, ChemistrySelect , 10 (2025) 33. https://doi.org/10.1002/slct.202503075

[6] Z. Ur Rahman, U. Shah, A. Alam, Z. Shah, K. Shaheen, S. Bahadar Khan, S. Ali Khan, Photocatalytic degradation of cefixime using CuO–NiO nanocomposite photocatalyst, Inorg. Chem. Commun. , 148 (2023)

110312.https://doi.org/10.1016/j.inoche.2022.110312

[7] S. Sezer, P. Demircivi, N. Erdol Aydin, G. Nasun Saygili, Photocatalytic degradation of ciprofloxacin using tannin-doped $BaTiO_3$ catalyst, J. Photochem. Photobiol. A: Chem., 451 (2024) 115604.https://doi.org/10.1016/j.jphotochem.2024.115468

[8] Y. Jia, Y. Zhang, X. Zhang, J. Cheng, Y. Xie, Y. Zhang, X. Yin, F. Song, H. Cui, Novel CdS/PANI/MWCNTs photocatalysts for photocatalytic degradation of xanthate in wastewater, Sep. Purif. Technol., 309 (2023) 122992.https://doi.org/10.1016/j.seppur.2022.123022